coatings

MDPI

Article

Ammonia Plasma Surface Treatment for Enhanced Cu–Cu Bonding Reliability for Advanced Packaging Interconnection

Ho Jeong Jeon and Sang Jeen Hong *

Department of Semiconductor Engineering, Myongji University, 116 Myoungjiro, Yongin 17058, Republic of Korea; 04jhj1120@naver.com

* Correspondence: samhong@mju.ac.kr; Tel.: +82-31-330-6374

Abstract: With the emergence of 3D stacked semiconductor products, such as high-bandwidth memory, bonding-interface reliability cannot be overemphasized. The condition of the surface interface before bonding is important and can substantially affect product reliability. Plasma technology can be used to control the state of a bonding interface, but various factors of interest, such as surface roughness, chemical bonding state, and surface cleanliness, may depend on the type of gaseous plasma. These factors may increase voids at the interface, which can jeopardize the product reliability. In this study, NH_3 plasma surface treatment is investigated and compared with the conventionally preferred surface treatment under Ar plasma. Under the latter method, specific anomalies occurred and led to void formation at the interface during bonding. By contrast, NH_3 plasma treatment maintained higher uniformity, higher overall surface conditions, and a smooth reduction process. Furthermore, the formation of a nitride passivation layer effectively inhibited the oxidation of the metal surface, and the flat surface resulted in the decrease in voids compared with the Ar plasma treatment after the copper–copper bonding. From the experimental analysis, we achieved a 12% reduction in resistance in the samples treated with NH_3 plasma treatment due to the suppression of surface oxidation. However, it is unfortunate that the shear strength in the experimental samples treated with NH_3 plasma treatment needs to be further improved.

Keywords: 3D stack; Cu–Cu bonding; plasma; surface treatment; reliability

check for updates

Citation: Jeon, H.J.; Hong, S.J. Ammonia Plasma Surface Treatment for Enhanced Cu–Cu Bonding Reliability for Advanced Packaging Interconnection. *Coatings* **2024**, *14*, 1449. https://doi.org/10.3390/coatings14111449

Academic Editor: Shih-Nan Hsiao

Received: 13 October 2024
Revised: 9 November 2024
Accepted: 12 November 2024
Published: 14 November 2024

Copyright: © 2024 by the authors. Licensee MDPI, Basel, Switzerland. This article is an open access article distributed under the terms and conditions of the Creative Commons Attribution (CC BY) license (https://creativecommons.org/licenses/by/4.0/).

1. Introduction

The needs for excellent device density, high signal communication bandwidth, superior performance, and low manufacturing costs persist with the expansion of the role of 3D packaging in the field of semiconductors [1,2]. An example of early 3D packaging technology is stacked chip-scale packaging with copper wires, but an increase in the number of copper wires in a package leads to a power consumption problem, signal loss, and the increased package footprint [3]. Through-silicon vias (TSVs) have been devised to alleviate concerns of multiple wire bonding, but the high cost of TSV fabrication on wafers has hindered the emergence of the application in commercial products [4]. Likewise, direct Cu–Cu bonding with TSV interconnection is a promising interconnection method in 3D packaging [5]. Cu–Cu bonding involves connecting two copper bumps or pads back-to-back in a TSV to interconnect another semiconductor chip, and it can also be used for hybrid bonding along with SiO_2–SiO_2 bonding [6]. It plays a crucial role in advanced packaging, a stacked high-bandwidth memory (a type of dynamic random-access memory), and backside power delivery networks [7,8].

Cu–Cu bonding technology is currently being investigated in various research directions. Cu–Cu bonding is normally conducted at temperatures exceeding 400 °C. Its thermal impact on nearby components can be reduced by decreasing the bonding temperature. This can be achieved via surface-activated bonding using plasma surface treatment [9]. Additionally, various issues related to the bonding interface are being studied, including

oxidation and diffusion problems [10,11]. Papers on oxidation problems focus on inhibiting oxidation itself and removing oxide layers through plasma and wet chemical surface treatments. As for diffusion problems, researchers are investigating the application of coatings to the copper surface to promote diffusion during bonding [12–16]. Plasma technology should be used effectively to address these challenges. Ar plasma–based surface treatment has been adopted in many studies; this process is driven by Ar ion sputtering, which physically removes the bond between copper and oxygen. Although this process performs well in surface activation and oxide film removal, it requires appropriate control because it may increase the surface roughness [17].

For successful Cu–Cu bonding, surface conditions should be controlled strictly. The key factors affecting surface conditions include surface roughness, surface chemical state, and surface cleanliness [18]. The surface roughness should be minimized, and any surface oxide layer must be removed. The presence of particles on the surface can disrupt proper bonding and reduce bonding reliability [19]. Plasma processes enable the control of these parameters. Surface roughness reduction decreases the probability of void formation during bonding and increases the contact area between different Cu surfaces, thereby improving the shear strength and electrical properties of devices [20]. The effective control of oxide layers can enhance electrical characteristics and copper atom diffusion. The roughness of a copper surface is improved by adding H_2 to Ar plasma during plasma surface treatment [17]. Furthermore, the use of N_2 plasma for copper surface treatment effectively suppresses oxidation by forming a passivation layer on the surface [21]. In this study, the copper surface treatment was performed using NH_3 plasma to obtain the passivation layer expected from N_2 plasma and the improved surface roughness expected from H_2 plasma. In the following section, we explain how the samples were prepared, bonded, and tested, including the plasma surface treatment procedure. In Section 3, we present our experimental results and discuss our observations regarding the bonding strength. Finally, the conclusion is presented in Section 4.

2. Experiment

2.1. Surface Activation

A total of 50 nm of Ti barrier layer and 1 µm of Cu film were deposited on a 4-inch Si wafer via physical vapor deposition. Plasma surface treatment was performed using the plasma-enhanced chemical vapor deposition (PECVD) equipment, as shown in Figure 1. The process recipes for the sample fabrication are presented in Table 1. Ar plasma primarily facilitated a physical process. Ar gas is considered an unreactive gas, as it does not readily react with other elements. This characteristic makes Ar suitable for processes involving sputtering, where physical effects dominate. In this physical bombardment process, we achieved a reduced oxidized surface, shown in Figure 2a. Unlike Ar plasma, NH_3 plasma was selected not for a physical effect but for its chemical effect, which minimized physical damage to the copper surface presented in Figure 2b [22,23]. Hydrogen and nitrogen radicals formed within the NH_3 plasma. When the hydrogen radicals reacted with the surface oxygen the copper oxide layer was removed from the surface. Then the removal proceeds to the interface of Cu/Cu_2O, then slowly moves from the surface region and, at last, the entire whole metallic layer is reduced [24]. After the reduction process, nitrogen-free radicals generated by N_2 plasma reacted chemically with pure copper atoms, devoid of oxygen, resulting in the formation of copper nitride. This copper nitride acted as a passivation layer, preventing copper oxidation before Cu–Cu bonding, thus protecting the copper surface [25].

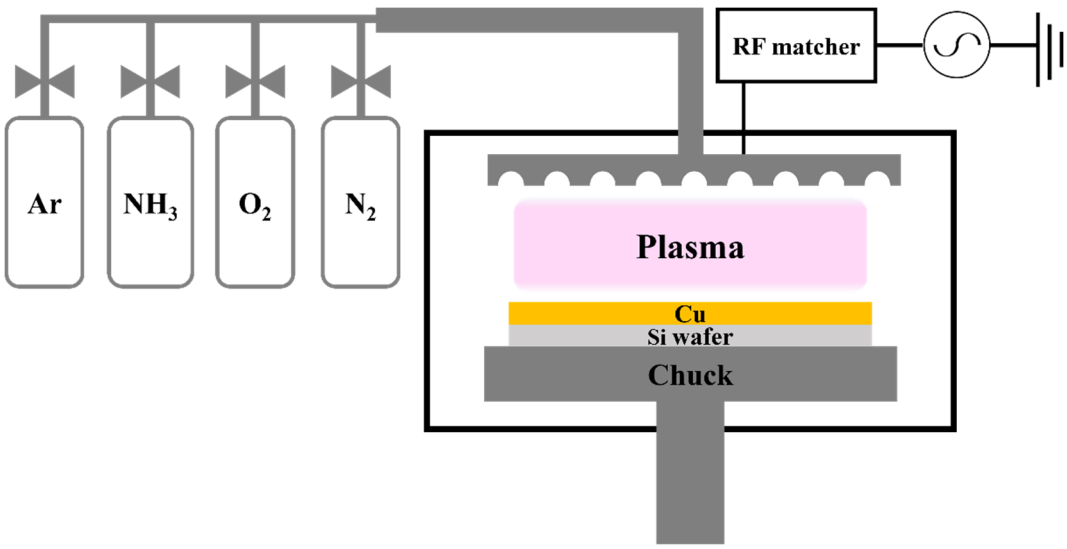

Figure 1. A schematic diagram of the 13.56 MHz CCP-type PECVD used in the experiment.

Table 1. Plasma surface treatment feasibility test.

Sample Number	Gas	Power (W)	Flow Rate (sccm)	Pressure (Torr)	Time (s)
1	Ar	300	50	1	30
2	NH_3 (50%)/Ar	300	NH_3 25/Ar 25	1	30
3	NH_3 (90%)/Ar	300	NH_3 45/Ar 5	1	30

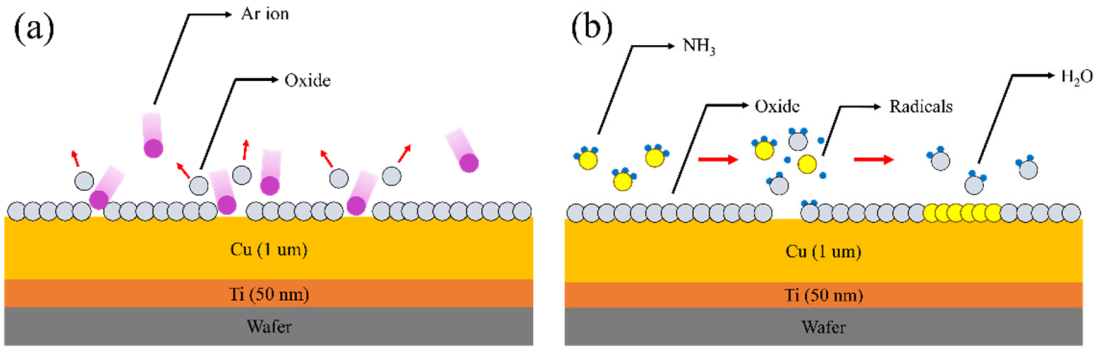

Figure 2. Schematics of Ar plasma and NH_3 plasma effect on copper oxide: (**a**) physical effect of Ar plasma; (**b**) chemical effect of NH_3 plasma.

2.2. Bonding Process

Cu–Cu bonding was conducted via thermal compression bonding (TCB), which involves the application of heat and pressure. The bonding process was carried out as shown in Figure 3.This bonding process was conducted at 420 °C for 1 h, followed by an additional annealing process at 400 °C for 30 min. Cu–Cu bonding using heat and pressure typically comprises three stages. The initial stage (plastic deformation) occurs at the peaks of a wavy surface, followed by diffusion within the voids between the bonded surfaces. This diffusion leads to the formation of grain boundaries. Finally, the voids at the bonding interface ripen, thus completing the bonding process [26]. The additional annealing process was conducted for stronger bonding [27].

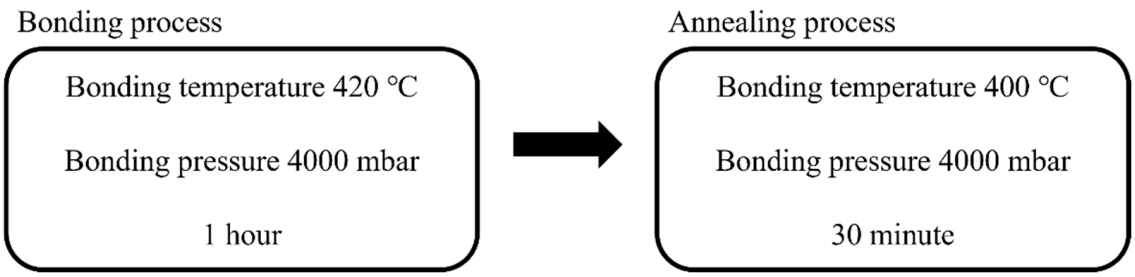

Figure 3. Two-step process flow chart of Cu–Cu bonding.

3. Results and Discussion

3.1. Atomic Force Microscopy (AFM) Analysis of Cu Surface

After surface treatment using plasma, atomic force microscopy (AFM) was used to evaluate the state of the Cu surface. The AFM results were analyzed in terms of different characteristics: line roughness, surface roughness, and AFM peaks. Line roughness and surface roughness are expressed by the parameters R_a and R_q. R_a represents the arithmetic mean of the deviation in height from the measured data's average height, while Rq is the root mean square of the variation in height across the surface profile. Both values are used to characterize surface roughness. For line roughness analysis, measurements were obtained at various positions. However, the measured results do not consistently exhibit a specific trend. Some measured line roughness values are high at certain positions, whereas others are low. This inconsistency shows that line roughness analysis is unsuitable for this study. The next roughness parameter considered was surface roughness, which represented the roughness value throughout the measurement area. Roughness is expected to increase after Ar plasma treatment; by contrast, in this study, surface roughness does not significantly differ between the samples treated using Ar plasma and NH_3 plasma, as observed in Figure 4a,b. However, other parameters exhibit significant differences. Figure 4c,d depict the data for the height of the highest peak from the reference plane throughout the measured total area (R_p), and the sum of the highest peak and the deepest valley across the measured total area (R_y), respectively. As shown in the graphs in Figure 4c,d, as the NH_3 content increases, R_p and R_y decrease. This phenomenon is also evident in the 3D AFM image in Figure 5. This finding is attributed to a partial, irregular phenomenon indicating the high peaks forming on the reference plane resulting from the argon sputtering effect, and implies that the likelihood of this phenomenon decreases with the influence of Ar during plasma treatment. Furthermore, this partial, irregular phenomenon may increase the probability of void formation between the bonded surfaces during bonding.

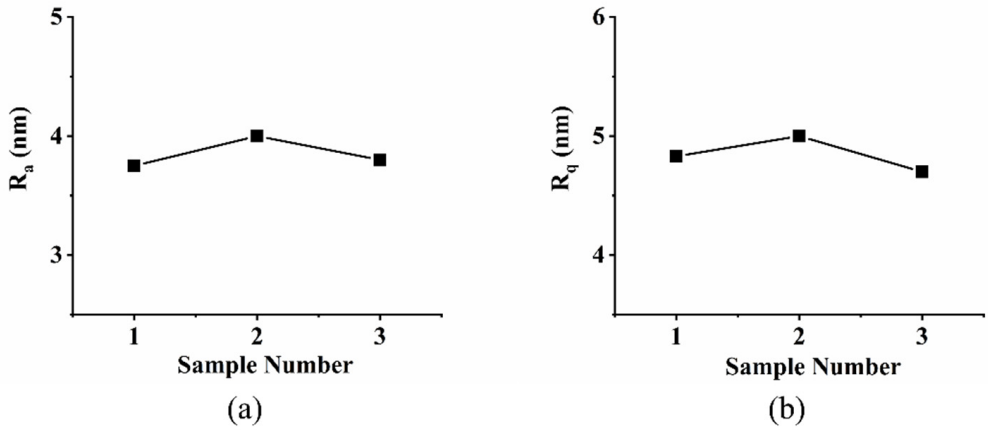

Figure 4. *Cont.*

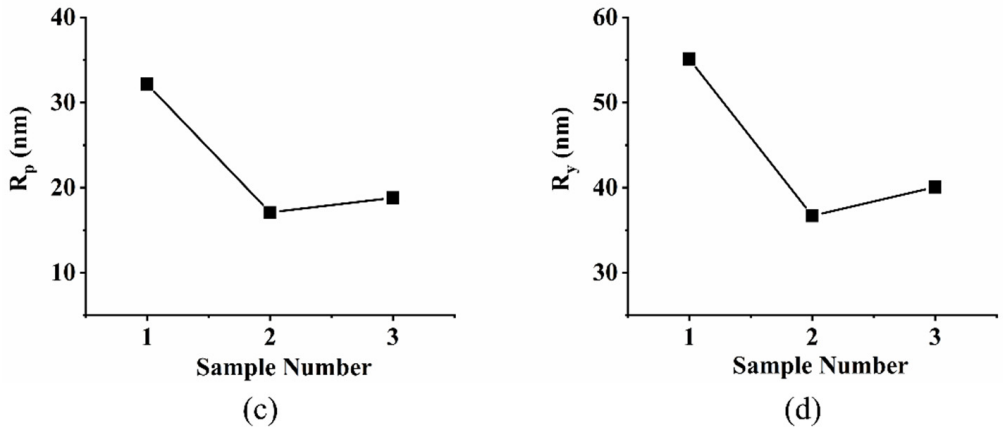

Figure 4. Results of Cu surface roughness after plasma surface treatment: (**a**) roughness data presented by R_a; (**b**) roughness data presented by R_q; (**c**) roughness data presented by R_p; (**d**) roughness data presented by R_y.

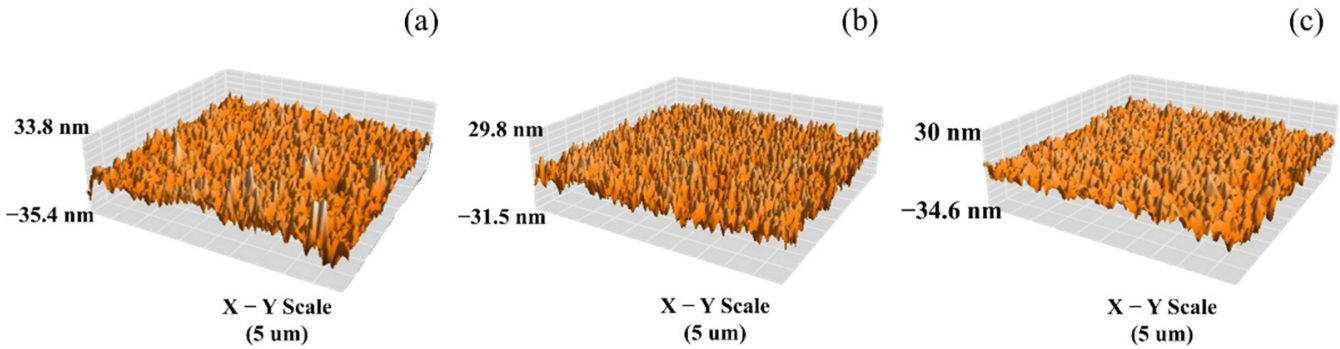

Figure 5. Surface 3D image inspected by AFM after surface treatment: (**a**) 100% of Ar plasma; (**b**) 50% of NH_3 with 50% of Ar plasma; (**c**) 90% of NH_3 plasma with 10% of Ar plasma.

3.2. X-Ray Photoelectron Spectroscopy (XPS) Analysis of Cu Surface

We investigate the chemical bonding state of the surface based on the type of plasma used through XPS analysis. In Figure 6, the Cu $2p_{3/2}$ peaks for the processes involving different types of plasma are evident. The peak at 932.2 eV corresponds to pure Cu, indicating the absence of oxidation or nitridation. The peak at 933.8 eV is associated with CuO [28,29]. As for the process using NH_3 plasma, the surface consists of nitride caused by the chemical reactions of the nitride radicals generated in the NH_3 plasma, resulting in the formation of Cu_3N [30]. The Cu_3N peak is observed at 933.2 eV in Figure 6b,c [31]. For the O1s peak, as shown in Figure 7, dominant wavelengths are observed between 529 eV and 531 eV. At 529.9 eV and 530.8 eV, Cu_2O and CuO are identified, respectively [32,33]. The significant reduction observed with NH_3 plasma treatment confirms visible improvement in overall oxide levels. Hence, recipes 1 and 3 from Table 1 were selected for the process, considering the substantial improvement in oxide levels achieved through NH_3 plasma treatment, as confirmed visually. In Figure 8, the N1s spectra, not observed in the Ar plasma process, are seen, and they increase with the NH_3 ratio. This confirms the presence of nitride components on the surface and can be inferred to be a passivation layer that prevents oxidation.

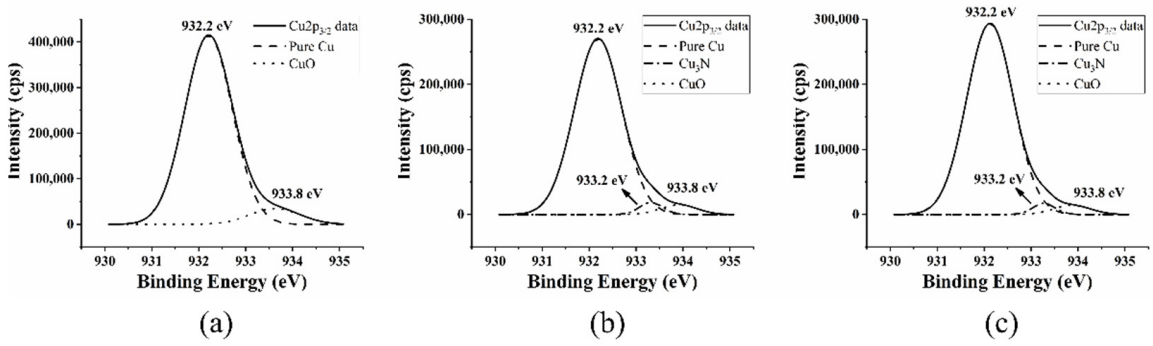

Figure 6. XPS $Cu2p_{3/2}$ spectra treated with different plasma: (**a**) 100% of Ar plasma; (**b**) 50% of NH_3 with 50% of Ar plasma; (**c**) 90% of NH_3 plasma with 10% of Ar plasma.

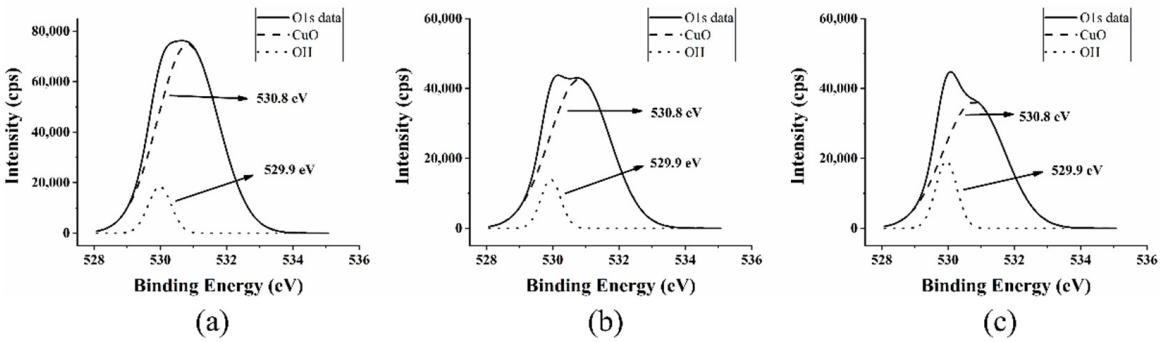

Figure 7. XPS O1s spectra treated with different plasma: (**a**) 100% of Ar plasma; (**b**) 50% of NH_3 with 50% of Ar plasma; (**c**) 90% of NH_3 plasma with 10% of Ar plasma.

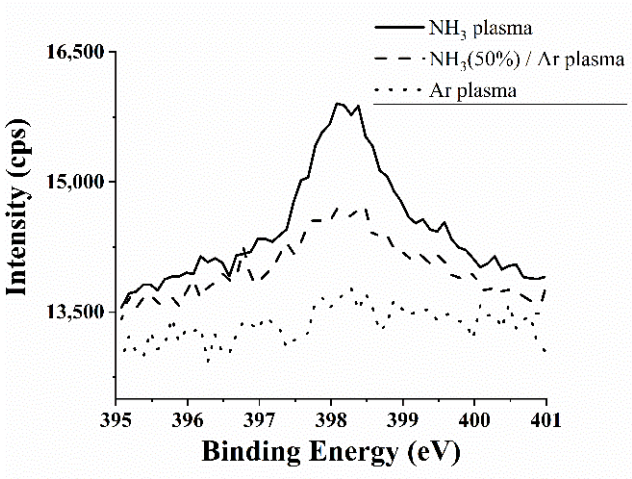

Figure 8. XPS N1s spectra treated with different plasma.

3.3. Scanning Acoustic Microscopy (SAM) Analysis

Following the TCB process, void inspection was conducted using scanning acoustic microscopy (SAM). In the SAM images in Figure 9, the dark regions represent well-bonded areas, whereas the bright regions indicate poor bonding. Differences in the bright areas, which represent voids, are observed between Figure 9a,b. As for the shades of the dark regions, the image in Figure 9b, which involves the formation of the nitride passivation layer, is brighter than that in Figure 9a. This difference is likely due to the possibility of the improper decomposition of copper nitrides during bonding. A single SAM image is insufficient for comparison, so additional electrical and physical experiments, such as

current–voltage (I–V) and shear tests, were conducted to assess the reliability of the bonded copper effectively.

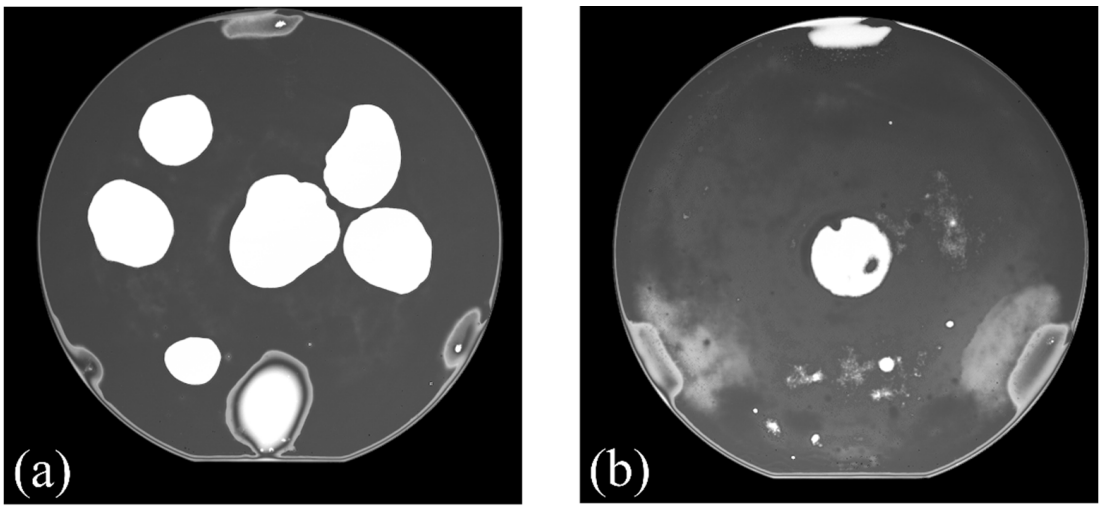

Figure 9. SAM data of Cu surface: (**a**) Ar plasma surface treatment before Cu–Cu bonding; (**b**) NH_3 plasma surface treatment before Cu–Cu bonding.

3.4. I–V Test

I–V tests were conducted to investigate the electrical characteristics of the bonded copper. I–V test samples were prepared as shown in Figure 10. To conduct the I–V test, after dicing the bonded copper samples, we applied silver paste to each end of the samples to establish an electrical connection between the copper and the measuring equipment. These tests were performed to utilize the deposited Cu layer as a metal layer and examine the electrical properties of the wiring. The I–V test results are in Figure 11. Resistance was calculated by dividing the applied voltage by the measured current. A comparison of the resistances obtained using this method shows that the samples treated using NH_3 plasma have lower resistance compared with those treated using Ar plasma. However, this result cannot be solely attributed to the difference between the pure Cu and the Cu surface with a passivation layer, as oxidation occurred during sample preparation. Relative to the Ar plasma process, the NH_3 plasma process is more effective in inhibiting oxidation, resulting in lower resistance in the oxidized Cu.

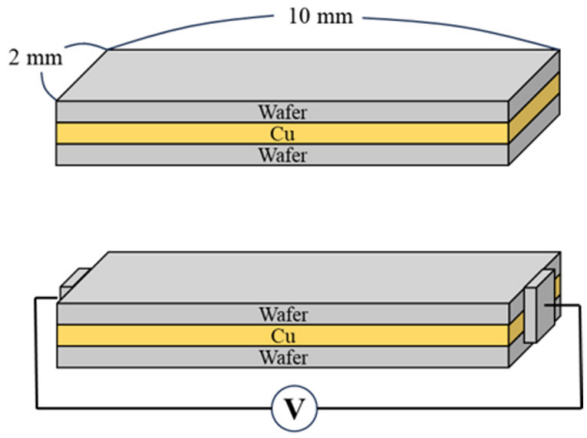

Figure 10. Schematic of sample used in I–V test.

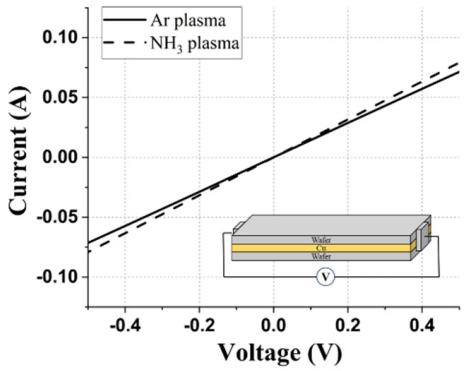

Figure 11. I–V curve of sample differ by plasma.

Simulations were conducted to validate the I–V test method. The sample shown in Figure 10 is represented as an equivalent circuit in Figure 12. We represent the resistances of the materials. For example, the resistance of wafer is represented as R_{wafer} and Ti is R_{Ti}. The resistance of copper (R_{Cu}) was calculated and used in the simulation by regarding the previously obtained resistance as R_{total} and applying it to the parallel resistor formula. The simulation results are shown in Figure 13.

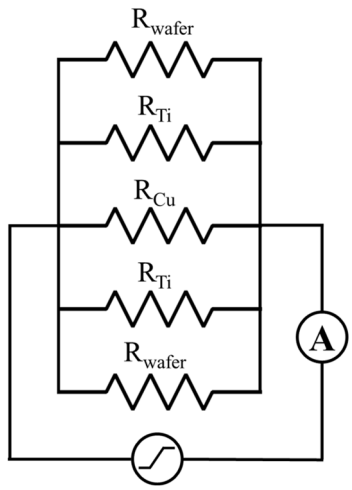

Figure 12. Equivalent circuit of sample used in I–V test.

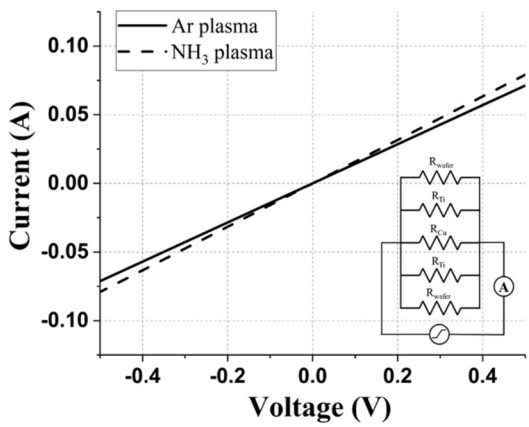

Figure 13. I–V test simulation data of Cu–Cu bonding samples using Ar plasma and NH_3 plasma.

3.5. Shear Test

For the bonding strength measurement, experiments where force is applied horizontally, such as shear tests, are more appropriate than experiments where force is applied

vertically to the bonding interface, such as four-point bending tests. Samples sized 2 × 2 mm^2 were prepared for our shear tests. Equation (1) was used for the precise measurement of bonding strength [34].

$$\tau = \frac{F_{\text{failrue}}}{A} \tag{1}$$

In the above equation, τ represents the shear strength, F_{failure} corresponds to the force at which the bond is broken, and A denotes the area of the shear test specimen. Shear tests were conducted following the method shown in Figures 14 and 15. The results in Figure 16 show that Cu–Cu bonding using Ar plasma exhibits a higher shear strength compared with Cu bonding using NH_3 plasma. The passivation layer formed when using NH_3 plasma should decompose at temperatures exceeding 350 °C [35]. However, during the bonding process in this study, the copper nitride passivation layer was insufficiently decomposed, leading to bonding in the form of copper nitride. Consequently, the bonding strength under the use of NH_3 plasma is lower than under the use of Ar plasma. This issue has also been observed in other experiments. Therefore, additional research may be necessary for the effective removal or decomposition of the passivation layer when conducting Cu–Cu bonding with such layers.

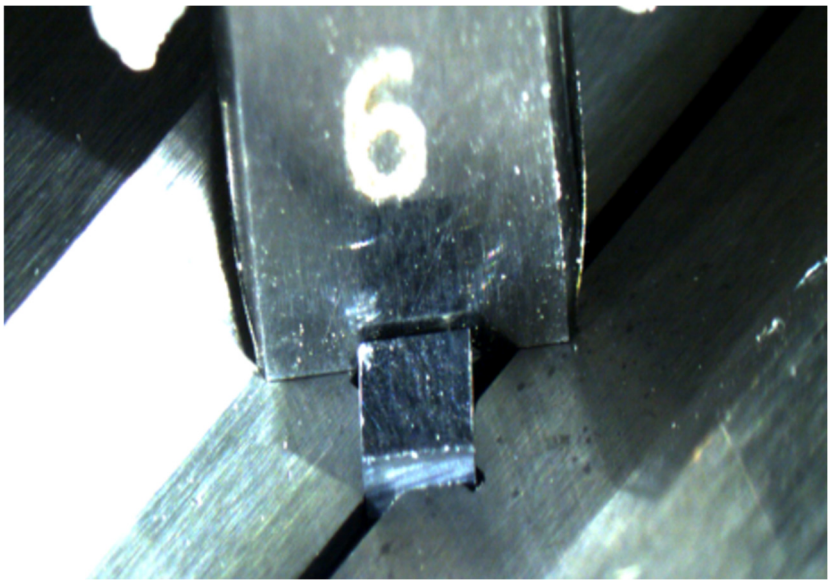

Figure 14. Image of Cu–Cu bonding shear test.

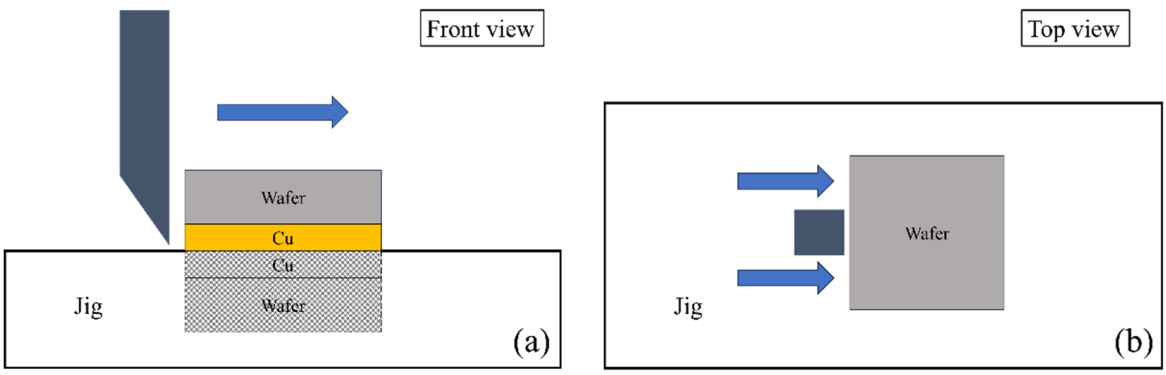

Figure 15. Explanation schematic of Cu–Cu bonding shear test: (**a**) front view of Cu–Cu bonding shear test; (**b**) top view of Cu–Cu bonding shear test.

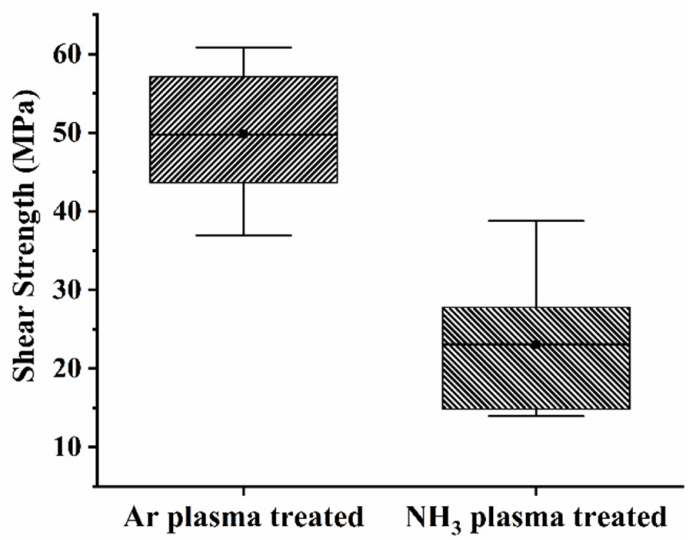

Figure 16. Shear test results of Cu–Cu bonded samples.

3.6. Transmission Electron Microscopy (TEM) Analysis

A TEM analysis of Cu–Cu bonding was conducted for surface treatment using Ar plasma and surface treatment using NH_3 plasma, which is presented in Figure 17. For treatment using Ar plasma, voids are discernible at the bonding interface. In contrast, for treatment using NH_3 plasma, the bonding interface is hardly distinguishable, and the defects readily identified as voids in Figure 17a are not easily visible in Figure 17b. The image in Figure 18 schematically represents the shape of Figure 17a, clearly showing the presence of voids. This observation can be related to the AFM findings. According to the roughness findings in Figures 4 and 5 and the 3D AFM image, during surface treatment using Ar plasma, nonideal peaks and valleys formed, unlike during treatment using NH_3 plasma. The initiation of bonding in this state may lead to the formation of significant gaps at the bonding interface, thus increasing the probability of void formation. This explains why more voids emerged during treatment using Ar plasma.

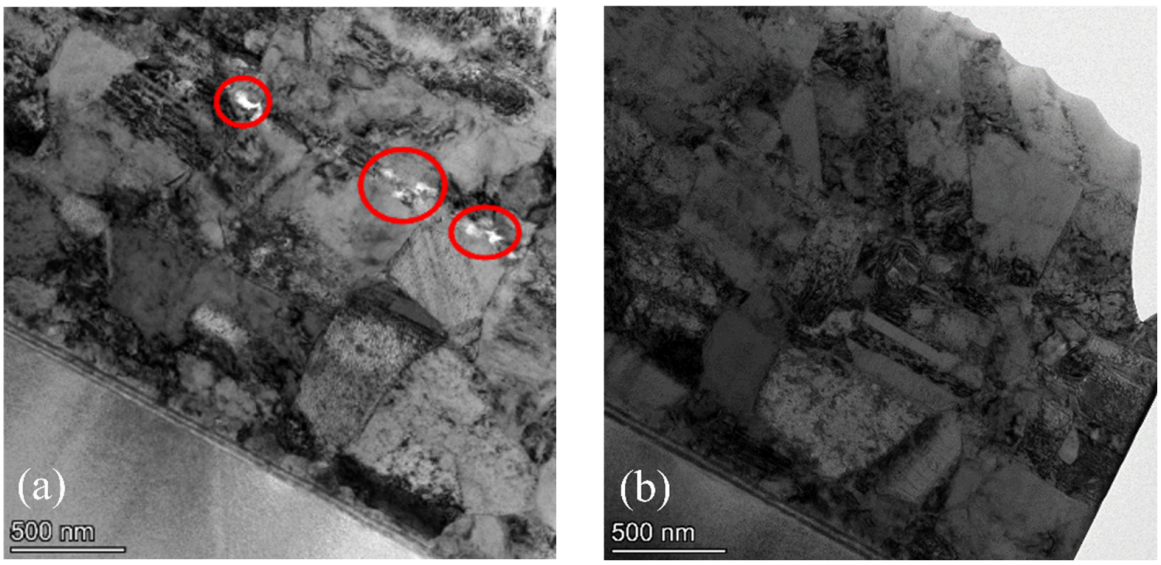

Figure 17. TEM analysis of Cu–Cu bonding: (**a**) using Ar plasma surface treatment; (**b**) using NH_3 plasma surface treatment.

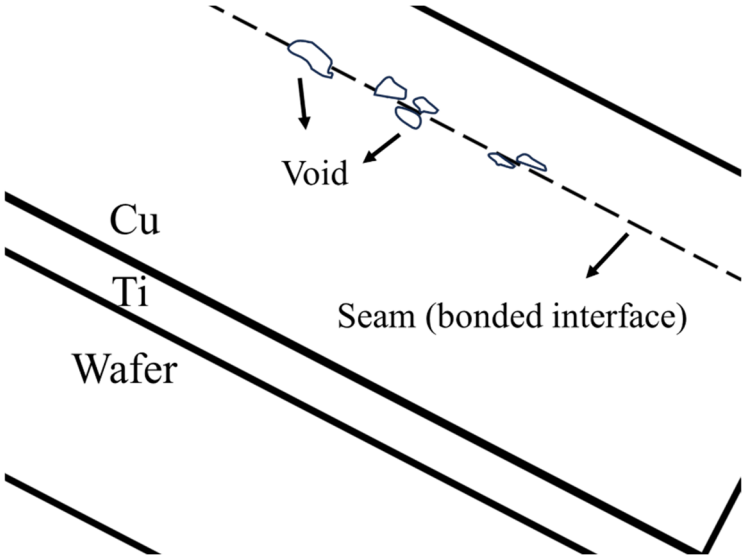

Figure 18. Schematic of Cu–Cu bonding TEM image explaining seam and voids followed by Figure 17a.

4. Conclusions

In this study, we investigated the effects of using Ar plasma and NH_3 plasma for Cu surface treatment during Cu–Cu bonding via TCB. We found that these treatments influenced the inhibition of oxidation and the suppression of void formation. The passivation layer formed during NH_3 plasma surface treatment played a significant role in inhibiting oxidation. Moreover, the plasma surface treatment mechanism had a substantial impact on the suppression of void formation. We compared the physical effects dominant in Ar plasma surface treatment, where physical processes prevailed, with the chemical reactions predominant in NH_3 plasma surface treatment. Notably, we observed significant differences in the surface roughness parameters R_p and R_y, with NH_3 plasma surface treatment, which exhibited smaller values of R_p and R_y, resulting in fewer voids. However, Ar plasma surface treatment led to higher bonding strength. This was attributed to the insufficient decomposition of the passivation layer formed during NH_3 plasma surface treatment. This incomplete decomposition compromised the bonding strength, resulting in Cu nitride–Cu nitride bonding rather than Cu–Cu bonding. In semiconductor manufacturing, where the production of a single semiconductor product consumes considerable time, copper oxidation should be inhibited. However, the passivation layer formed during NH_3 plasma surface treatment must eventually be removed to improve the electrical and physical properties of the product. In this study, the insufficiently decomposed passivation layer compromised the physical properties of the product. Therefore, in future research, the impact of this passivation layer should be minimized for improved performance.

Author Contributions: Conceptualization, S.J.H.; experiment and analysis, H.J.J.; writing—original draft preparation, H.J.J. and S.J.H.; writing—review and editing, S.J.H.; visualization, H.J.J.; funding acquisition, S.J.H. All authors have read and agreed to the published version of the manuscript.

Funding: This research was supported by the Korea Evaluation & Planning Institute for Industrial Technology (GID: K_G012002249203).

Institutional Review Board Statement: Not applicable for studies not involving humans or animals.

Informed Consent Statement: Not applicable for studies not involving humans.

Data Availability Statement: The data presented in this study are available on request from the corresponding author. The data are not publicly available due to the restriction of the equipment supplier.

Acknowledgments: Authors are grateful to staff on Semiconductor Process Diagnosis Research Center at Myongji University for maintaining high-level equipment condition.

Conflicts of Interest: The authors declare no conflicts of interest.

References

1. Agarwal, R.; Cheng, P.; Shah, P.; Wilkerson, B.; Swaminathan, R.; Wuu, J.; Mandalapu, C. 3D Packaging for Heterogeneous Integration. In Proceedings of the 2022 IEEE 72nd Electronic Components and Technology Conference (ECTC), San Diego, CA, USA, 31 May–3 June 2022; pp. 1103–1107. [CrossRef]
2. Agarwal, R.; Kannan, S.; England, L.; Reed, R.; Song, Y.; Lee, W.; Lee, S.; Yoo, J. 3D Packaging Challenges for High-End Applications. In Proceedings of the 2017 IEEE 67th Electronic Components and Technology Conference (ECTC), Orlando, FL, USA, 30 May–2 June 2017; pp. 1249–1256. [CrossRef]
3. Oh, B.H.; Loo, H.Y.; Oh, P.T.; Lee, E.K. Challenges in Stacked CSP Packaging Technology. In Proceedings of the 2006 International Conference on Electronic Materials and Packaging, Kowloon, China, 11–14 December 2006; pp. 1–4. [CrossRef]
4. Tian, Y.; Fang, H.; Ren, N.; Zhao, Y.; Chen, B.; Wu, F.; Paik, K.-W. Reliable Single-Phase Micro-Joints with High Melting Point for 3D TSV Chip Stacking. *J. Alloys Compd.* **2020**, *828*, 154468. [CrossRef]
5. Suga, T.; He, R.; Vakanas, G.; La Manna, A. Direct Cu to Cu Bonding and Alternative Bonding Techniques in 3D Packaging. In *3D Microelectronic Packaging: From Architectures to Applications*; Li, Y., Goyal, D., Eds.; Springer Series in Advanced Microelectronics; Springer: Singapore, 2021; pp. 201–231. ISBN 9789811570902.
6. Kagawa, Y.; Fujii, N.; Aoyagi, K.; Kobayashi, Y.; Nishi, S.; Todaka, N.; Takeshita, S.; Taura, J.; Takahashi, H.; Nishimura, Y.; et al. An Advanced CuCu Hybrid Bonding for Novel Stacked CMOS Image Sensor. In Proceedings of the 2018 IEEE 2nd Electron Devices Technology and Manufacturing Conference (EDTM), Kobe, Japan, 13–16 March 2018; pp. 65–67. [CrossRef]
7. Gao, G.; Mirkarimi, L.; Fountain, G.; Suwito, D.; Theil, J.; Workman, T.; Uzoh, C.; Guevara, G.; Lee, B.; Huyhn, M.; et al. Low Temperature Hybrid Bonding for Die to Wafer Stacking Applications. In Proceedings of the 2021 IEEE 71st Electronic Components and Technology Conference (ECTC), San Diego, CA, USA, 1 June–4 July 2021; pp. 383–389. [CrossRef]
8. Nagano, F.; Inoue, F.; Phommahaxay, A.; Peng, L.; Chancerel, F.; Naser, H.; Beyer, G.; Uedono, A.; Beyne, E.; Gendt, S.D.; et al. Origin of Voids at the SiO_2/SiO_2 and SiCN/SiCN Bonding Interface Using Positron Annihilation Spectroscopy and Electron Spin Resonance. *ECS J. Solid State Sci. Technol.* **2023**, *12*, 033002. [CrossRef]
9. Kim, T.; Howlader, M.; Itoh, T.; Suga, T. Room Temperature Cu–Cu Direct Bonding Using Surface Activated Bonding Method. *J. Vac. Sci. Technol. Vac. Surf. Films* **2003**, *21*, 449–453. [CrossRef]
10. Park, M.; Baek, S.; Kim, S.; Kim, S.E. Argon Plasma Treatment on Cu Surface for Cu Bonding in 3D Integration and Their Characteristics. *Appl. Surf. Sci.* **2015**, *324*, 168–173. [CrossRef]
11. Tanaka, K.; Wang, W.-S.; Baum, M.; Froemel, J.; Hirano, H.; Tanaka, S.; Wiemer, M.; Otto, T. Investigation of Surface Pre-Treatment Methods for Wafer-Level Cu-Cu Thermo-Compression Bonding. *Micromachines* **2016**, *7*, 234. [CrossRef] [PubMed]
12. Kim, Y.; Park, S.; Kim, S.E. Effect of Ag Nanolayer in Low Temperature Cu/Ag-Ag/Cu Bonding. *J. Microelectron. Packag. Soc.* **2021**, *28*, 59–64.
13. Bonam, S.; Panigrahi, A.K.; Kumar, C.H.; Vanjari, S.R.K.; Singh, S.G. Interface and Reliability Analysis of Au-Passivated Cu–Cu Fine-Pitch Thermocompression Bonding for 3-D IC Applications. *IEEE Trans. Compon. Packag. Manuf. Technol.* **2019**, *9*, 1227–1234. [CrossRef]
14. Huang, Y.-P.; Chien, Y.-S.; Tzeng, R.-N.; Shy, M.-S.; Lin, T.-H.; Chen, K.-H.; Chiu, C.-T.; Chiou, J.-C.; Chuang, C.-T.; Hwang, W.; et al. Novel Cu-to-Cu Bonding with Ti Passivation at 180 °C in 3-D Integration. *IEEE Electron Device Lett.* **2013**, *34*, 1551–1553. [CrossRef]
15. Panigrahi, A.K.; Bonam, S.; Ghosh, T.; Vanjari, S.R.K.; Singh, S.G. High Quality Fine-Pitch Cu-Cu Wafer-on-Wafer Bonding with Optimized Ti Passivation at 160 °C. In Proceedings of the 2016 IEEE 66th Electronic Components and Technology Conference (ECTC), Las Vegas, NV, USA, 31 May–3 June 2016; pp. 1791–1796. [CrossRef]
16. Panigrahi, A.K.; Ghosh, T.; Vanjari, S.R.K.; Singh, S.G. Demonstration of Sub 150 °C Cu-Cu Thermocompression Bonding for 3D IC Applications, Utilizing an Ultra-Thin Layer of Manganin Alloy as an Effective Surface Passivation Layer. *Mater. Lett.* **2017**, *194*, 86–89. [CrossRef]
17. Hsieh, J.; Fong, L.; Yi, S.; Metha, G. Plasma Cleaning of Copper Leadframe with Ar and Ar/H_2 Gases. *Surf. Coat. Technol.* **1999**, *112*, 245–249. [CrossRef]
18. Tang, Y.-S.; Chang, Y.-J.; Chen, K.-N. Wafer-Level Cu–Cu Bonding Technology. *Microelectron. Reliab.* **2012**, *52*, 312–320. [CrossRef]
19. Chen, K.-N.; Tan, C.; Fan, A.; Reif, R. Copper Bonded Layers Analysis and Effects of Copper Surface Conditions on Bonding Quality for Three-Dimensional Integration. *J. Electron. Mater.* **2005**, *34*, 1464–1467. [CrossRef]
20. Gondcharton, P.; Imbert, B.; Benaissa, L.; Verdier, M. Voiding Phenomena in Copper-Copper Bonded Structures: Role of Creep. *ECS J. Solid State Sci. Technol.* **2015**, *4*, P77. [CrossRef]
21. Seo, H.; Park, H.S.; Kim, S.E. Two-Step Plasma Treatment on Sputtered and Electroplated Cu Surfaces for Cu-to-Cu Bonding Application. *Appl. Sci.* **2019**, *9*, 3535. [CrossRef]
22. Chang, Y.-M.; Leu, J.; Lin, B.-H.; Wang, Y.-L.; Cheng, Y.-L. Comparison of H_2 and NH_3 Treatments for Copper Interconnects. *Adv. Mater. Sci. Eng.* **2013**, *2013*, 1–7. [CrossRef]
23. Ito, F.; Shobha, H.; Tagami, M.; Nogami, T.; Cohen, S.; Ostrovski, Y.; Molis, S.; Maloney, K.; Femiak, J.; Protzman, J.; et al. Effective Cu Surface Pre-Treatment for High-Reliable 22 Nm-Node Cu Dual Damascene Interconnects with High Plasma Resistant Ultra Low-k Dielectric (K = 2.2). *Microelectron. Eng.* **2012**, *92*, 62–66. [CrossRef]

24. Gong, Z.; Zhong, W.; He, Z.; Liu, Q.; Chen, H.; Zhou, D.; Zhang, N.; Kang, X.; Chen, Y. Regulating Surface Oxygen Species on Copper (I) Oxides via Plasma Treatment for Effective Reduction of Nitrate to Ammonia. *Appl. Catal. B Environ.* **2022**, *305*, 121021. [CrossRef]
25. Park, H.; Seo, H.; Kim, S.E. Anti-Oxidant Copper Layer by Remote Mode N2 Plasma for Low Temperature Copper–Copper Bonding. *Sci. Rep.* **2020**, *10*, 21720. [CrossRef]
26. Shie, K.-C.; Gusak, A.; Tu, K.-N.; Chen, C. A Kinetic Model of Copper-to-Copper Direct Bonding under Thermal Compression. *J. Mater. Res. Technol.* **2021**, *15*, 2332–2344. [CrossRef]
27. Jang, E.-J.; Kim, J.-W.; Kim, B.; Matthias, T.; Park, Y.-B. Annealing Temperature Effect on the Cu-Cu Bonding Energy for 3D-IC Integration. *Met. Mater. Int.* **2011**, *17*, 105–109. [CrossRef]
28. Wu, C.-K.; Yin, M.; O'Brien, S.; Koberstein, J.T. Quantitative Analysis of Copper Oxide Nanoparticle Composition and Structure by X-Ray Photoelectron Spectroscopy. *Chem. Mater.* **2006**, *18*, 6054–6058. [CrossRef]
29. Kautek, W.; Gordon, J.G. XPS Studies of Anodic Surface Films on Copper Electrodes. *J. Electrochem. Soc.* **1990**, *137*, 2672. [CrossRef]
30. Noguchi, J.; Ohashi, N.; Yamaguchi, H.; Takeda, K. Dependence of Time-Dependent Dielectric Breakdown Lifetime on NH_3-Plasma Treatment in Cu Interconnects. *Jpn. J. Appl. Phys.* **2005**, *44*, 4859. [CrossRef]
31. Yu, A.; Hu, R.; Liu, W.; Zhang, R.; Zhang, J.; Pu, Y.; Chu, L.; Yang, J.; Li, X. Preparation and Characterization of Mn Doped Copper Nitride Films with High Photocurrent Response. *Curr. Appl. Phys.* **2018**, *18*, 1306–1312. [CrossRef]
32. Wang, J.; Li, C.; Zhu, Y.; Boscoboinik, J.A.; Zhou, G. Insight into the Phase Transformation Pathways of Copper Oxidation: From Oxygen Chemisorption on the Clean Surface to Multilayer Bulk Oxide Growth. *J. Phys. Chem. C* **2018**, *122*, 26519–26527. [CrossRef]
33. Sreedharan, R.; Mohan, M.; Saini, S.; Roy, A.; Bhattacharjee, K. Intermediate Cu-O-Si Phase in the Cu-SiO_2/Si (111) System: Growth, Elemental, and Electrical Studies. *ACS Omega* **2021**, *6*, 23826–23836. [CrossRef]
34. Seo, H.; Park, H.S.; Kim, G.; Park, Y.-B.; Kim, S.E. Bonding Strength Evaluation of Copper Bonding Using Copper Nitride Layer. *J. Microelectron. Packag. Soc.* **2020**, *27*, 55–60. [CrossRef]
35. Wang, D.; Nakamine, N.; Hayashi, Y. Properties of Various Sputter-Deposited Cu–N Thin Films. *J. Vac. Sci. Technol. Vac. Surf. Films* **1998**, *16*, 2084–2092. [CrossRef]

Disclaimer/Publisher's Note: The statements, opinions and data contained in all publications are solely those of the individual author(s) and contributor(s) and not of MDPI and/or the editor(s). MDPI and/or the editor(s) disclaim responsibility for any injury to people or property resulting from any ideas, methods, instructions or products referred to in the content.